

# Hofmeister effect for electrokinetic transport at ordered DNA layers

Qianqian Cao<sup>1,2</sup>

Received: 16 February 2016 / Accepted: 31 August 2016 / Published online: 8 September 2016  
© Springer-Verlag Berlin Heidelberg 2016

**Abstract** Development of DNA nanotechnology provides the basis to construct novel biomimetic DNA nanochannels. In this work, we report electrokinetic transport behavior of the fluid through the surfaces consisting of double-stranded DNA molecules based on all-atom molecular dynamics simulations. The results show that an electric double layer forms close to the DNA surface, and the fluid can be driven by an externally applied electric field. At large DNA–DNA separation, a velocity jump is observed when the electric field is exerted along the direction of the central axis of DNA. Increasing the DNA separation does not influence the flow velocity in the model parameters investigated. It was also found that the magnitude of electroosmotic flow velocity obeys the Hofmeister series.

## 1 Introduction

Natural nanochannels are a family of biological membrane proteins, which play a critical role in controlling exchange of specific ions and molecules inside and outside of cells (Hille 2001). In general, polar molecules and charged ions are allowed to passively migrate through the channels down the electrochemical gradient without direct expenditure of metabolic energy. Biological nanochannels possess high selectivity, conductivity and sensitivity in controlling ionic and molecular transport. For example, the throughput

of potassium ions through potassium nanochannels is four orders of magnitude higher than sodium ions (Doyle et al. 1998). Inspired by biomembrane nanochannels, the construction and development of artificial nanochannels have received growing attention (Dekker 2007; Hou et al. 2011; Sakai and Matile 2013; Hernández-Ainsa and Keyser 2014). In the last two decades, a large number of nanochannels with various functions, such as biosensing, flow controlling and single molecule detection, are fabricated experimentally. Research in the field of bio-inserted artificial nanochannels provides the possibility to study many biological processes in vitro and to develop potential applications in bionanotechnology and nanomedicine.

Implementation of functionalities of the nanochannels mainly depends on the physicochemical properties of the surfaces, the channel shape and dimension. Artificial nanochannel systems may be constructed directly from natural nanochannels or fabricated by drilling pores into solid-state inorganic substrates (Li et al. 2001; Dekker 2007), such as polymer membrane, silicon-based material and graphene. For example, a natural nanochannel can be inserted into a reconstituted lipid membrane to implement the in vitro detection of single biomolecules (Kasianowicz et al. 1996). Such nanochannels have some distinct advantages similarly to membrane ion channels. However, they are susceptible to external environment, and have unadjustable shape and size. Solid-state nanochannels can overcome these disadvantages, but their sensitivity and control accuracy are much lower in molecular detection compared to natural nanochannels. For these solid-state channels, it is difficult to achieve high transport performance as natural protein channels which approach the diffusional limit. A strategy to overcome these limitations consists of combining robustness and adjudication of solid-state nanochannels with biological functions of natural nanochannels. As a result,

✉ Qianqian Cao  
qqcao@mail.zjxu.edu.cn

<sup>1</sup> College of Mechanical and Electrical Engineering, Jiaying University, Jiaying 314001, People's Republic of China

<sup>2</sup> Fachbereich Physik, Freie Universität Berlin, 14195 Berlin, Germany

hybrid channels were achieved by inserting natural nanochannels or biomolecule-based nanochannels into solid-state channels (Hall et al. 2010).

Based on DNA origami nanotechnology, a long single-stranded DNA can be folded by adding a number of short DNA molecules with complementary sequences to form a predefined nanostructure with precise shape and dimension (Rothemund 2006). Recently, several groups have used this bottom-up technology to generate innovative DNA nanochannels, such as hybrid DNA origami solid-state nanochannels (Bell et al. 2012; Hernández-Ainsa et al. 2014) and membrane-spanning DNA nanochannels (Langecker et al. 2012; Burns et al. 2013; Seifert et al. 2015). These channels exhibit fascinating performance in single molecule detection, and open a new field to mimic biological ion nanochannels due to tunable size, stability, reversibility and programmability of DNA origami. Additionally, chemical modifiability of DNA with atomic accuracy and its electrochemical sensitivity are expected to lead to a broader range of exciting applications. Furthermore, the DNA origami nanotechnology also makes design and manufacture of nanochannels easier because the DNA nanostructures can be predicted exactly using available computer softwares (Douglas et al. 2009).

Unlike solid-state channels where discreteness of surface charges and microscopic corrugation of the surface play an important role in controlling hydrodynamic and electrostatic friction (Kim and Netz 2006), small ions and water can permeate into the surfaces of the DNA channels. Moreover, it is also different from channels coated with polymer brushes which have much softer surfaces and deform more easily when environmental parameters are altered. We have studied electrokinetic transport behavior of the fluid through nanochannels modified with neutral polymer brushes (Cao et al. 2010, 2011) and polyelectrolyte brushes (Cao et al. 2012). Electrical double layer (EDL) can be influenced by polymer layers, and there exists strong coupling between conformational dynamics of polymer chains and transport dynamics of the fluid. Luan and Aksimentiev have performed the first all-atom molecular dynamics (MD) study of electrokinetic transport of DNA in a solid nanopore (Luan and Aksimentiev 2008). Recently, Li et al. (2015) studied ionic conductivity and structural deformation of DNA origami in external electric field by means of MD simulations. Their results demonstrate that MD simulations can be used as a predictive tool to explore the properties of synthetic DNA nanostructures. The all-atom MD methods have been also used to investigate various electrokinetic phenomena of DNA systems, such as the effect of ion valence (Luan and Aksimentiev 2010), the differential effect of monovalent cations (Kowalczyk et al. 2012), the temperature effect (Belkin and Aksimentiev 2016) and the electrokinetic effects in DNA membrane channels (Yoo

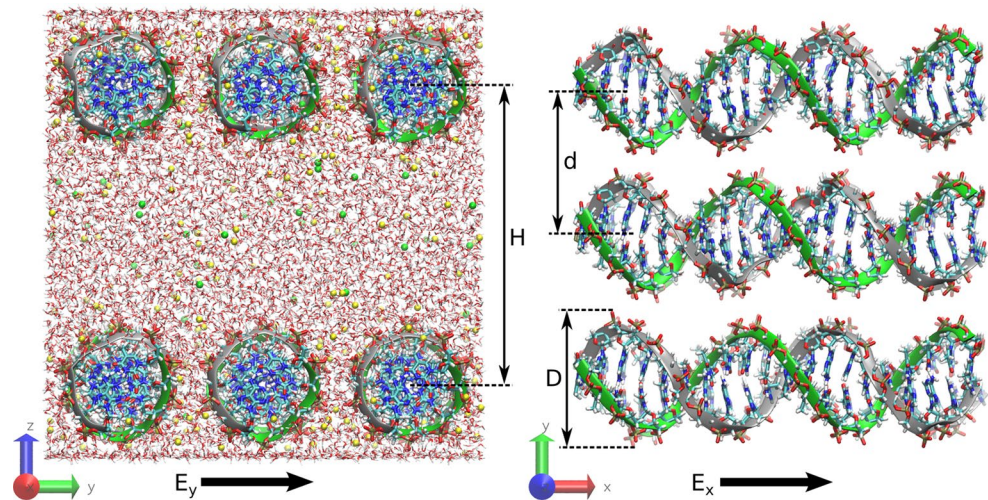
and Aksimentiev 2015). In this work, all-atom MD simulations are employed to simulate the electrokinetic transport of fluid confined between two opposing DNA surfaces. The MD method provides physical insight at the atomic level into the transport mechanism of ions and water molecules through the DNA surface. We do not take into account short DNA strands linking two adjacent DNAs. The purpose of our work is to understand how the charged DNA surface influences the flow characteristics of confined fluid and the ion distribution near the rough surfaces. The effects of the ion specificity, channel width, separation between neighboring DNAs and direction of electric field are also addressed.

## 2 Model and simulation method

The particles in the system are confined by two Lennard–Jones 9-6 potential walls along the  $z$  direction. The average separation between each potential wall and adjacent DNA surface is about 0.4 nm. Each DNA surface layer consists of two or three double-stranded(ds) DNA molecules depending on the gap of  $d$  between each other. Two parallel DNA surfaces are set at distance  $H$  from each other. A typical simulation snapshot is shown in Fig. 1 to illustrate the simulation system. Each DNA chain contains 20 base pairs. The positions of the DNA surfaces are constrained by harmonic restraint potentials with spring constant  $600 \text{ kJ mol}^{-1} \text{ nm}^{-2}$  acting on each phosphorus atom. All DNA chains are completely periodic, that is, a phosphodiester bond between the terminal 3'-hydroxyl group and 5'-phosphate group in each single-stranded DNA traverses the periodic simulation box. In this work, a common set of cations including  $\text{Cs}^+$ ,  $\text{Rb}^+$ ,  $\text{K}^+$ ,  $\text{Na}^+$ ,  $\text{Li}^+$ ,  $\text{Ca}^{2+}$  and  $\text{Mg}^{2+}$  are used to elucidate the influence of ion-specific effect on transport dynamics, and the corresponding anions  $\text{Cl}^-$  are added. Counterions are added to neutralize the negative charges on two DNA surfaces. Additional salt concentration is fixed at 0.15 M for monovalent (54 cations, 54  $\text{Cl}^-$ ) and divalent cases (54 cations, 108  $\text{Cl}^-$ ). The number of water molecules in the box changes from 6500 to 25,000 depending on  $H$ .

The Lennard–Jones (LJ) potential is truncated at 1 nm. A switching function is used between 0.85 nm and the cut-off distance to make the forces decay smoothly to zero. Water molecules are modeled by using the SPC/E model (Berendsen et al. 1987). We use the LINCS algorithm to constrain the water geometry (Hess et al. 1997). The long-range electrostatic interactions are treated by the particle-method Ewald (PME) method with a real-space cutoff of 1.1 nm (Darden et al. 1993). Periodic boundary conditions are applied in all three directions. To remove the periodicity in the  $z$  direction normal to the wall, an empty

**Fig. 1** Illustration of the simulation system for electrokinetic transport of fluid through DNA surfaces. The *left picture* shows the cross section of the model. Each surface includes three dsDNA chains orientated parallel to each other. The *right sketch* gives the top view for a single surface (only DNA chains are shown). All snapshots are generated using VMD (Humphrey et al. 1996)



volume with the height of  $3L_z$  is inserted along the  $z$  direction, where the  $z$ -directional dimension of the box is set to  $L_z = H + D + 0.8$  nm. The average diameter  $D$  of the dsDNA molecules is about 2.1 nm.

The Gromacs software package (Spoel et al. 2005) is used for calculating all bonding and nonbonding interactions. The force field parameters for DNA molecules and ions are based on the Amber99 force field (Wang et al. 2000). However, the parametrization of nucleic acid systems can cause artifacts due to ion aggregation, in particular for divalent cations that bind directly to the phosphate oxygens of DNA. Therefore, two optimized parameter sets from Yoo and Aksimentiev (2012), Yoo et al. (2016), and Mamatkulov et al. (2013) are also used to simulate the systems containing  $Mg^{2+}$  and  $Ca^{2+}$ . We abbreviate these two types of parameterizations to FFY for the former and FFM for the latter. It is worth emphasizing that the custom models of hydrated ions in FFY are introduced. For example, seven water molecules are restrained to a  $Ca^{2+}$  ion, and six water molecules for a  $Mg^{2+}$  ion. The TIP3P and SPC/E water models are employed in simulations based on FFY and FFM, respectively.

To obtain the box size along the  $z$  direction at desired pressure, we first carried out a NPT simulation for 2 ns after energy minimization. The NPT simulation was performed under constant pressure  $P = 1$  bar by semi-isotropic box rescaling with fixed area  $A = L_x \times L_y$  and constant temperature  $T = 300$  K using Berendsen's method with a coupling time constant of 1 ps for pressure and 0.1 ps for temperature (Berendsen et al. 1984). After the NPT simulation, the average box size  $L_z$  along the  $z$  direction is calculated. Then, a NVT simulation for 8 ns runs under an applied external electric field to induce an electroosmotic flow. Finally, we perform a 30 ns simulation to collect data for the steady flow. Here, two different directions of the electric field along the  $x$  ( $E_x$ ) and  $y$  ( $E_y$ ) axes were considered,

respectively. The equations of motion are integrated using the leap-frog algorithm with a time step of 2 fs.

### 3 Results and discussion

We first focus on the equilibrium distributions of water molecules and ions. Figure 2c shows the density of water at different separation  $d$  between adjacent DNA chains at fluid surface separation  $H$ . The water density near the center of the DNA layer is reduced. Obviously, a decrease in  $d$  leads to a lower water density. There exists no significant oscillation in the interface between the DNA surface and the bulk solution. In contrast, for bare solid-state surfaces, the interaction between water and surface can induce large density oscillation. The rough DNA surface smooths out the distribution of interfacial water density. From simulation snapshots (Fig. 2a, b), it is seen that water molecules intrude into about 2/3 of the radius of DNA. In the central region of DNA, no water is observed. It is difficult to drive the water molecules inside DNA in the presence of stress. These waters exert lighter friction also to waters close to bulk solution. Therefore, the roughness of DNA, produced by major and minor grooves, suppresses significantly water flow.

The  $Na^+$  counterions are adsorbed near the charged DNA surface, and thus, an electrical double layer is formed. Additionally, some  $Na^+$  ions are also bound to the grooves of single DNAs and penetrate into gaps between adjacent DNA molecules (see snapshots in Fig. 2). Figure 3 shows the concentration profiles of  $Na^+$  and  $Cl^-$  ions and simulation snapshots for different channel widths at fixed  $d = 2.5$  nm. For the narrow channel with  $H \approx 5.1$  nm, the ion concentration exhibits peaks at the center of the channel, and a minimum in the concentration appears at the center of each DNA surface. There is a higher concentration



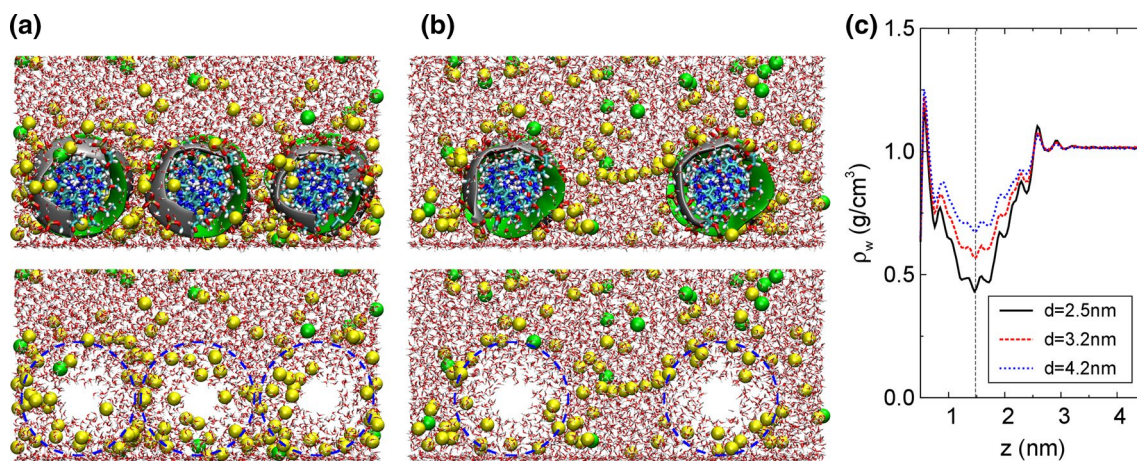


**Fig. 2** Snapshots in **a** and **b** correspond to DNA–DNA separation  $d = 2.5$  and  $4.2$  nm, respectively. DNA molecules are not shown in *bottom panel*. The *blue dashed circles* represent approximate size of DNA cross section. *Yellow and green beads* denote  $\text{Na}^+$  and  $\text{Cl}^-$  ions.

**c** Water density for different separation  $d$ . The *vertical line* represents the position of the central axis of DNA chains. The channel width is  $H \approx 10.4$  nm, and slightly changes depending on  $d$  (color figure online)

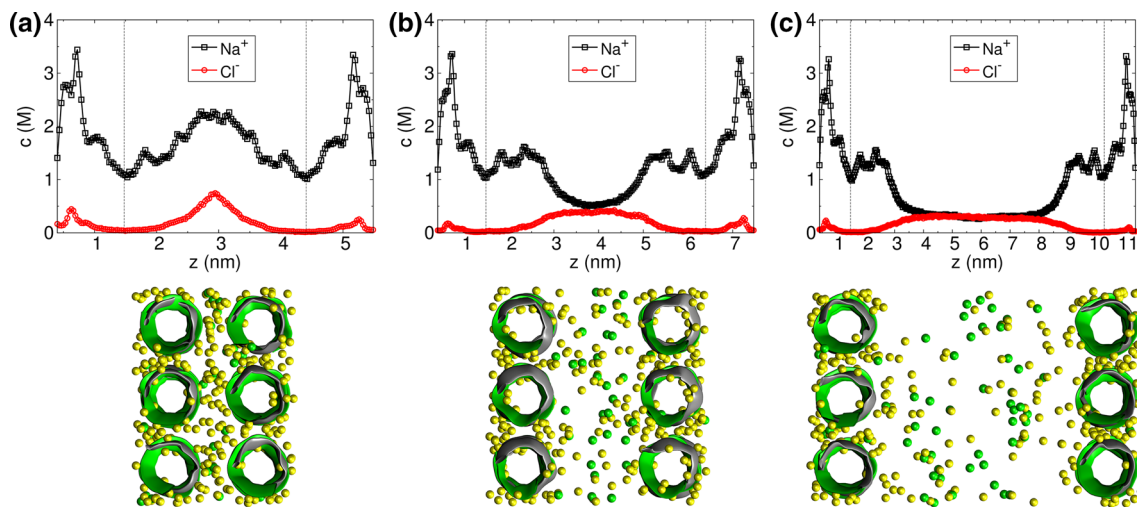


**Fig. 3** Ion concentration at different channel width **a**  $H \approx 5.1$  nm, **b**  $7.1$  nm, and **c**  $10.4$  nm. The DNA–DNA separation  $d$  is fixed at  $2.5$  nm. The *vertical lines* represent the position of the central axis of

DNA chains in each surface. The *snapshots from left to right on the bottom panel* correspond to the cases from **a** to **c**. Water is not shown

of  $\text{Na}^+$  ions compared to  $\text{Cl}^-$  ions. Doubtlessly, both electrical double layers for top and bottom surfaces overlap. With increasing channel width, the ion concentration at the channel center decreases to the bulk concentration. Additionally, the concentration of  $\text{Na}^+$  ions close to the DNA surfaces remains approximately constant. Most  $\text{Cl}^-$  ions are expelled from the interior of the surface. No ions can intrude into the region near the axial center of DNA. Note that many ions aggregate near potential walls because of dielectric effect.

Fluid can be driven due to the formation of electrical double layer when an electric field is applied along the

direction parallel to the DNA surface. Figure 4 shows the velocity profiles under external electric fields along the  $x$  and  $y$  directions. At the small separation  $d = 2.5$  nm, the flow velocity does not depend on the direction of electric field. In other words, it reveals that the difference in the distribution of surface charges along the  $x$  and  $y$  directions does not influence the flow velocity. The velocity of the fluid in the interior of the surface is suppressed significantly. The flow satisfies no-slip boundary conditions. Compared to a wider channel, the flow velocity at  $H \approx 5.1$  nm is lower and has a sharp peak in the center of the channel because of overlapped electrical double

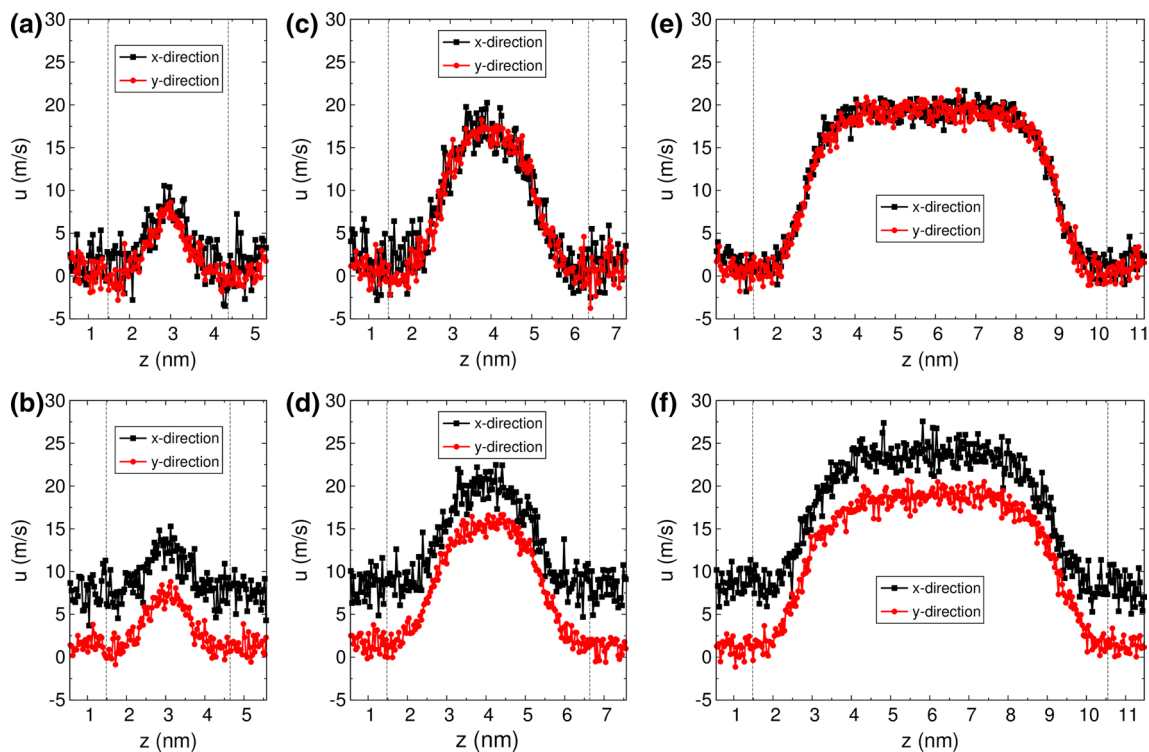


**Fig. 4** Electroosmotic flow velocity for different channel width  $H$  and DNA separation  $d$ . The channel width corresponds to  $H \approx 5.1$  nm, 7.1 nm, and 10.4 nm from left to right. The value of  $H$  slightly changes for different  $d$ . Top and bottom rows correspond to  $d = 2.5$  nm

and 4.2 nm, respectively. The velocity is measured along the  $x$  ( $E_x = 0.5$  V/nm and  $E_y = 0$ ) and  $y$  ( $E_x = 0$  and  $E_y = 0.5$  V/nm) directions. The vertical lines represent the position of the center of each DNA surface

layers. At  $H \approx 10.4$  nm, the velocity profile exhibits a well-defined plug-like shape.

Further, we investigate the flow velocity for the cases of a larger separation  $d = 4.2$  nm. Such separation between adjacent two dsDNA chains is able to accommodate only one dsDNA chain (Fig. 2b). It was found that the velocity is higher along the  $x$  direction. Clearly, nonzero velocity in the gap between neighboring DNA molecules causes the increase in the  $x$ -directional velocity. In the  $y$  direction, no velocity jump is observed. Moreover, the flow velocity along the  $y$  direction at the channel center is little affected by  $d$ . This means that zeta potential depends little on effective surface charges (Bonthuis and Netz 2012), indicating electrophoretic saturation effect. When the electric field is applied along the  $y$  direction perpendicular to the DNA axis, it is difficult to drive ions and water molecules between two adjacent DNA chains cross separate DNA chains. Therefore, the flow close to the surface is inhibited. For the applied electric field along the  $x$  direction, due to the absence of flow obstacles, the fluid between adjacent DNA chains can be driven. Further, the motion of the fluid drags water molecules near the surface to accelerate the fluid transport. At  $d = 2.5$  nm, the space between neighboring DNA chains is so small that the diffuse structure

of electrical double layer can not be formed. Therefore, the particles within the narrow gap are hardly dragged. At  $d = 4.2$  nm, the adjacent DNA chains have a gap of about 2 nm. There exists a diffuse layer for such gap, although an overlapping occurs.

To show the ion density within and near DNA surfaces more accurately, we plot two-dimensional ion concentration at  $H = 10.4$  nm in Fig. 5. The  $yz$  plane is chosen to calculate two-dimensional properties:  $\text{Na}^+$  concentration and velocity distribution (see below Fig. 6). There is a higher  $\text{Na}^+$  concentration between adjacent DNA molecules at  $d = 2.5$  nm. At larger separation of  $d = 4.2$  nm, the  $\text{Na}^+$  concentration becomes lower near the DNA molecules. Therefore, the decrease in separation promotes counterion condensation. It should be also noted that the electric double layers formed by single DNA molecules overlap as the inter-DNA distance is reduced. Changing the direction of electric field affects the distribution of ions in DNA surfaces. Obviously, the DNA molecules hinder movement of ions within the surface under electric field along the  $y$  direction. At narrow separation, when the  $y$ -directional field is applied, some  $\text{Na}^+$  ions are pushed into the DNA molecules. Unlike the case with the  $x$ -directional field, the most ions aggregate in the separation between adjacent DNA

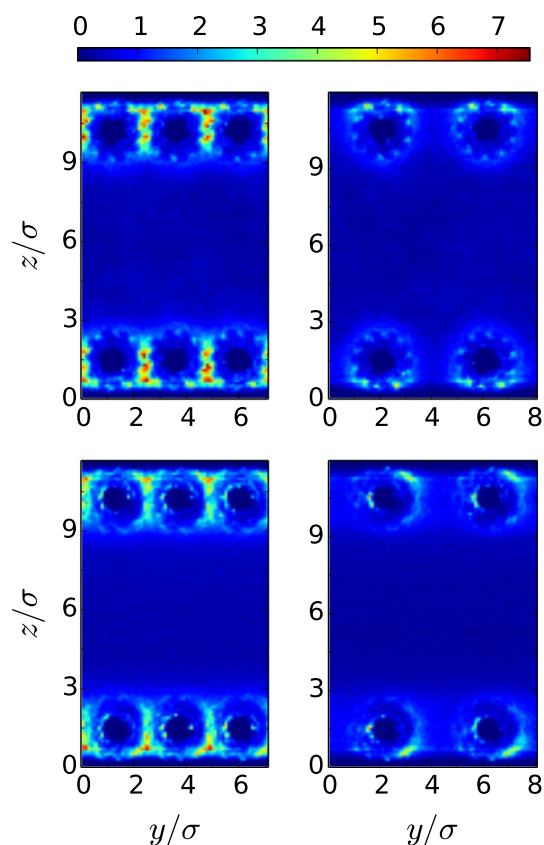


**Fig. 5** 2D  $\text{Na}^+$  ion concentration at (left)  $d = 2.5$  nm and (right)  $4.2$  nm. The channel width is  $H = 10.4$  nm. The electric field is applied along (top) the  $x$  and (bottom)  $y$  directions, respectively

molecules. For larger separation, the  $\text{Na}^+$  ions distribute around the DNA molecules at the  $x$ -directional field. The distribution of ions above the surface is smeared out under electric field along the  $y$  direction.

To examine the velocity distribution in entire channel and also explain the jump of flow velocity at large separation, we present the two-dimensional velocity distribution in Fig. 6. The flow velocity along the  $x$  and  $y$  directions corresponds to the  $x$ - (top) and  $y$ -directional (bottom) electric field, respectively. At small separation  $d = 2.5$  nm, the effect of the direction of electric field on the velocity distribution is negligible, except that the roughness of DNA molecules causes the fluctuations near the surface. At large separation  $d = 4.2$  nm, the change in the direction of electric field leads to remarkable variations in the velocity distribution. Unlike the small separation where the transport of fluid between neighboring DNA molecules is suppressed, the electroosmotic flow also generates in the region between adjacent DNA molecules. It is the main reason for the jump of velocity which appears in Fig. 5. When the electric field is exerted along the  $y$  direction, the separation nearly influences the velocity of fluid between

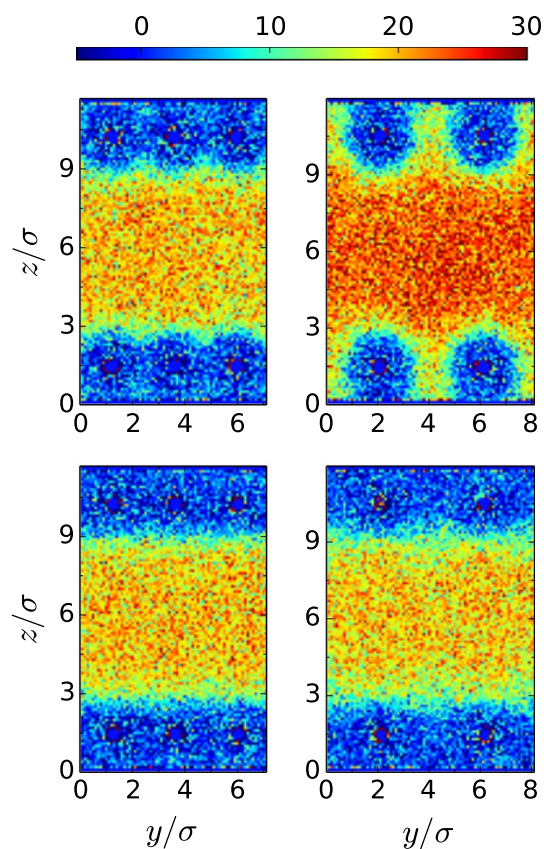


**Fig. 6** 2D electroosmotic flow velocity along (top) the  $x$  and (bottom)  $y$  directions, respectively. Other parameters are the same as those in Fig. 5

two DNA surfaces. The flow of fluid in the inter-DNA gap is shielded by DNA molecules perpendicular to the direction of electric field.

Studies on the interactions between DNA and cations have important implications for understanding the origin of DNA sequence-specific structural variations (Rouzina and Bloomfield 1998; Hud and Polak 2001; Saveliev and Papoian 2006). The binding ability of cations to DNA has a significant dependence on different ion types. Here, we explore the ion-specific effect on the transport of the fluid through the DNA surfaces. The specificity of various common cations, including  $\text{Cs}^+$ ,  $\text{Rb}^+$ ,  $\text{K}^+$ ,  $\text{Na}^+$ ,  $\text{Li}^+$ ,  $\text{Ca}^{2+}$  and  $\text{Mg}^{2+}$  with potential parameters based on Amber99 force field, is addressed. Figure 7 shows the ion-specific effect on the velocity profiles at fixed channel width and DNA separation. The flow velocity can be modulated by cationic specificity. The divalent  $\text{Ca}^{2+}$  and  $\text{Mg}^{2+}$  counterions strongly reduce the velocity due to strong electrostatic binding energy. Larger affinity for  $\text{Ca}^{2+}$  over  $\text{Mg}^{2+}$  toward binding to DNA has been observed in oriented fibers. However, the differences in bindings of these two cations become slight for gel electrophoresis under conditions



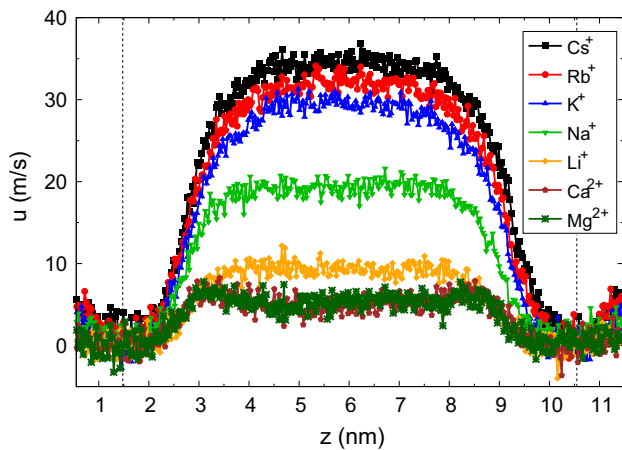
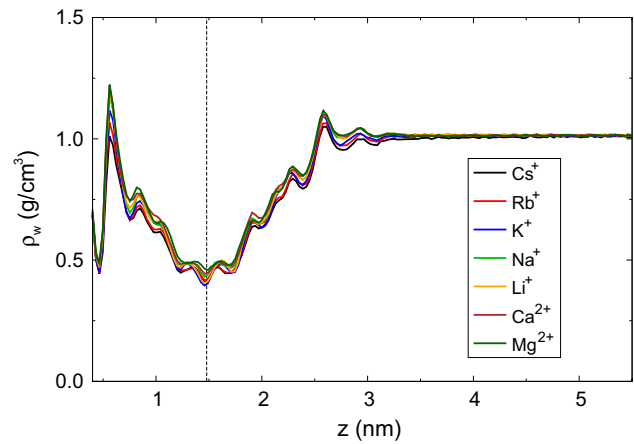


**Fig. 7** Electroosmotic flow velocity under electric field along the *y* direction for cases of different kinds of cations. The channel width and DNA separation are  $H = 10.4$  nm and  $d = 2.5$  nm, respectively. The vertical lines represent the position of the center of each DNA surface

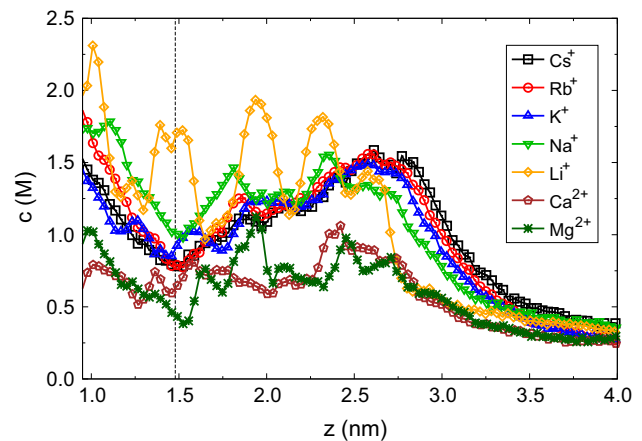
of aqueous solution (Li et al. 1998). Our results show the velocity profiles are almost coincident for  $\text{Ca}^{2+}$  and  $\text{Mg}^{2+}$  counterions. As a result, the binding differences for  $\text{Ca}^{2+}$  and  $\text{Mg}^{2+}$  ions have no major effect on the flow velocity. If the binding of counterions to DNA becomes much stronger, such as higher valent cations, the flow may be completely suppressed. For monovalent counterions, a standard Hofmeister series for the fluidic transport is identified. With changing cations from  $\text{K}^+$  to  $\text{Cs}^+$ , the increase in the velocity becomes slow in agreement with recent studies for carboxylates (Schwierz et al. 2015). Clearly, apart from the ion-specific effect, the flow is also dependent on the interaction between the surface and solvent molecules as well as interfacial solvent viscosity effect (Bonthuis and Netz 2012).

Figure 8 shows the density of water molecules for various kinds of cations. The water density in the interface (between 2.5 and 3 nm) is slightly lower for larger cations, such as  $\text{Cs}^+$  ion. This is because the larger cations have a higher concentration in the interface. For divalent cations, fewer amounts within the surface compared to monovalent ions result in a larger water density. We will further discuss the ion concentration below. As expected, the density of bulk water keeps constant.

Figure 9 presents the concentration profiles of different cations. Unlike channels with bare surfaces such as graphene or silicon surfaces, the ions spread into the DNA surface as discussed above. The increase in the cation concentration near the interface also obeys the Hofmeister series. For monovalent cations,  $\text{Li}^+$  ions have the strongest electrostatic correlation with DNA. Compared to other monovalent ions, the density of  $\text{Li}^+$  ions away from the DNA



**Fig. 8** Water density for cases of different kinds of cations. The model parameters are the same as those in Fig. 7. The vertical line represents the position of the center of the DNA surface



**Fig. 9** Concentrations of different kinds of cations. The model parameters are the same as those in Fig. 7. The vertical line represents the position of the center of the DNA surface

layer is much lower. Additionally, along the Hofmeister series, the density oscillation for monovalent cations within the DNA surface becomes larger. Because the degrees of freedom of DNA molecules are limited, the arrangement of atoms in DNA surfaces along the *z*-axis becomes more ordered. If a kind of cation binds more strongly to negative charges from DNA molecules, the oscillations in the cation density are also more remarkable in response to the arrangement of the DNA charges. Due to stronger binding ability for  $\text{Li}^+$ , the density peaks are more pronounced. As a consequence, the peaks become less pronounced along the series:  $\text{Li}^+$ ,  $\text{Na}^+$ ,  $\text{K}^+$ ,  $\text{Rb}^+$ ,  $\text{Cs}^+$ , as the binding ability lowers. For divalent cations, the number of cations bound to the DNA surfaces is less compared to monovalent cations. Therefore, the peaks do not enhance further. However,

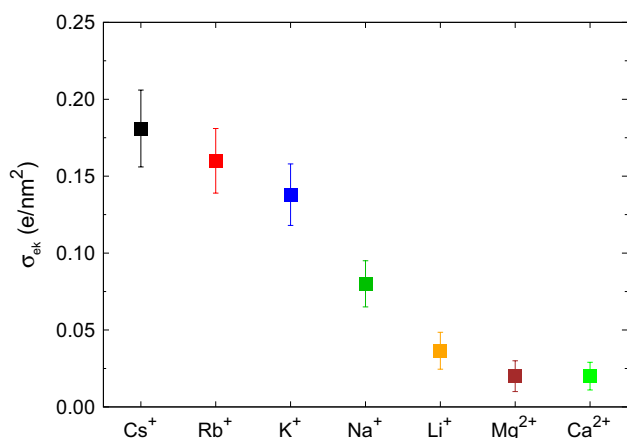


**Fig. 10** Electrokinetic surface charge density  $\sigma_{ek}$  for different kinds of cations. The model parameters are the same as those in Fig. 7

if the binding of divalent cations to DNA surfaces becomes stronger in specific force field as shown in Fig. 12, more pronounced peaks are also observed. Cl<sup>-</sup> ions are largely dissipated in the DNA layer regardless of cationic specificity because DNA is negatively charged (not shown here).

Based on the Grahame equation, we calculate the electrokinetic surface charge density  $\sigma_{ek}$  as an estimation of effective mobile surface charge density

$$\sigma_{ek} = \sqrt{\frac{8c_0\epsilon_0\epsilon_b}{\beta}} \sinh\left[\frac{\beta e\zeta}{2}\right] \quad (1)$$

where  $c_0$  is the bulk salt concentration,  $e$  is the elementary charge, and  $\beta = 1/k_B T$  with the Boltzmann constant  $k_B$ .  $\epsilon_0$  and  $\epsilon_b$  are the vacuum permittivity and the dielectric constant of bulk water at room temperature, respectively. The  $\zeta$ -potential is calculated using the Helmholtz–Smoluchowski equation

$$\lim_{z \rightarrow \infty} \frac{u_x(z)}{E_x} = -\frac{\epsilon_0\epsilon_b\zeta}{\mu_b} \quad (2)$$

with  $\mu_b = 0.642$  cP being the bulk viscosity for the SPC/E water model (Hess 2002). A similar value is also obtained in the study of interfacial water (Sendner et al. 2009). The bulk viscosity is much smaller compared to real water,  $\mu_b = 0.851$  cP (Weast 1986). Here,  $u_x(z)$  as  $z$  approaches infinity represents the average velocity of bulk fluid along the  $x$  direction in the central region of channel.

In Fig. 10, the electrokinetic surface charge density  $\sigma_{ek}$  is plotted according to the Hofmeister series. The results indicate that  $\sigma_{ek}$  has significant dependence on the ion-specific behavior. For the Cs<sup>+</sup> ions,  $\sigma_{ek} \approx 0.31$  e/nm<sup>2</sup>, which is about 12 times larger than that for divalent cations. Compared to the surface charge density  $\sigma_0 = 2.48$  e/nm<sup>2</sup> of the DNA layer,  $\sigma_{ek}$  is much lower. This is because a

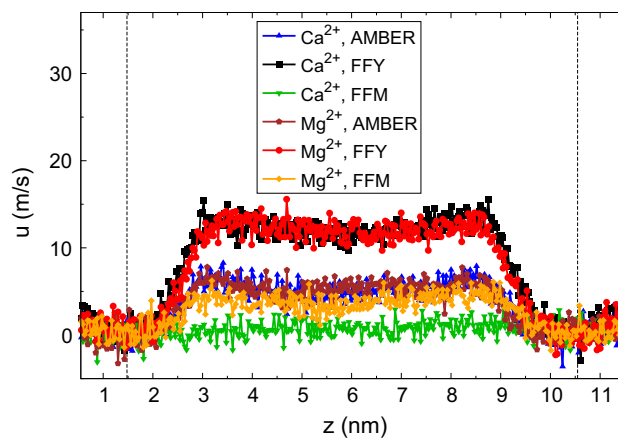


**Fig. 11** Electroosmotic flow velocity for Mg<sup>2+</sup> and Ca<sup>2+</sup> ions. The ion parameters are obtained from AMBER99 force field and recent works (Yoo and Aksimentiev 2012; Mamatkulov et al. 2013; Yoo et al. 2016). The channel width and DNA separation are  $H = 10.4$  nm and  $d = 2.5$  nm, respectively. The vertical lines represent the position of the center of each DNA surface

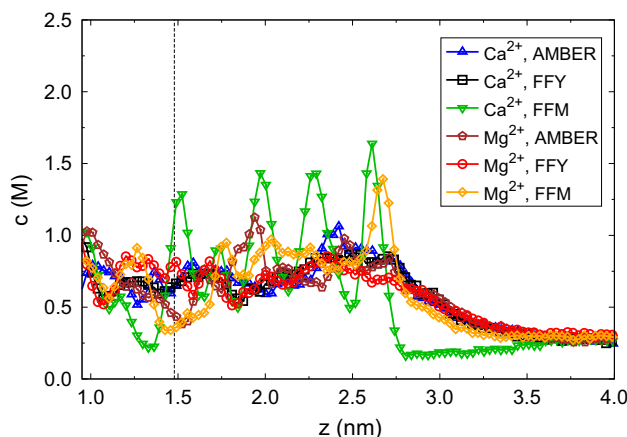


**Fig. 12** Ca<sup>2+</sup> and Mg<sup>2+</sup> ion concentrations. The model parameters are the same as those in Fig. 11. The vertical line represents the position of the center of the DNA surface

considerable amount of cations are captured in the minor or major grooves of DNA chains, which strongly limits the motion of cations. This is an extreme example of electrofriction which was previously shown to influence the electrophoretic mobility very sensitively. Experimentally (Lyklema 1995) and theoretically (Bonthuis and Netz 2012),  $\sigma_{ek}$  was found to saturate as a function of the bare surface charge density. In this work, when an electric field is applied along the  $y$  direction, in the case of Na<sup>+</sup> cations, the electroosmotic velocity is not affected as increasing  $d$  from 2.5 to 4.2 nm (Fig. 4). Therefore, the saturation behavior is also observed for soft DNA surfaces under model parameters investigated.



The commonly used force fields especially for divalent cations as implemented in AMBER and CHARMM may cause artifacts to describe ion-specific effects. Here, we make a comparison between three different force fields [original AMBER99, FFY (Yoo and Aksimentiev 2012; Yoo et al. 2016) and FFM (Mamatkulov et al. 2013)]. First, the flow velocity through the DNA surface is presented in Fig. 11. The FFY parameter set leads to larger velocity. Similarly to AMBER force field, no difference in velocity profiles for  $Mg^{2+}$  and  $Ca^{2+}$  ions is observed. The FFM developed by Mamatkulov et al. (2013) causes lower flow velocity. Moreover, the velocity profiles are not coincident for  $Mg^{2+}$  and  $Ca^{2+}$  ions. The reduced flow velocity means that the  $Ca^{2+}$  ions have stronger binding to negative charges of DNA. The  $Mg^{2+}$  ions bind more strongly its hydration shell and thus bind more weakly to negative charges of DNA (Mamatkulov et al. 2013). As seen from ion concentration profiles in Fig. 12, significant oscillations for the FFM parameter set also indicate strong affinity of divalent cations to DNA. In particular for  $Ca^{2+}$ , the ion concentration is much lower near the interface compared to other cases because more  $Ca^{2+}$  ions are bound into the DNA surface. For the FFY, there are no pronounced peaks in ion concentration profiles. The fine-tuned parameters in FFY can reproduce experimental osmotic pressure of binary electrolyte solutions of biologically relevant ions by increasing the LJ parameter  $\sigma$  that essentially weakens affinity between ions and phosphate oxygens of DNA. The parameters in FFM implies that the smaller  $Mg^{2+}$  ions bind more weakly to the halide ions than the larger  $Ca^{2+}$  ions, which can be demonstrated from experimental activity coefficients (Simonin et al. 2006). Such feature is also identified for the binding of ions to DNA in our simulations. Nevertheless, the binding ability for divalent cations in FFM is even stronger compared to AMBER force field. This is because the ion force field is optimized in salt solutions rather than bimolecular systems. The differences for different force fields suggest that it is necessary to make a correction to interaction parameters between divalent cations and biomolecules.

#### 4 Conclusions

In summary, we have explored the electrokinetic transport behavior of fluid confined between two DNA surfaces each of which consists of double-stranded DNA molecules in parallel arrangement using full-atom molecular dynamics simulations. We have examined the effects of various parameters on the flow characterization and the ion distribution. Our results show that not only the channel width  $H$  but also the gap  $d$  between adjacent DNA chains has an impact on the formation of the electrical double layer,

which is further relevant to the transport dynamics of the fluid. It is observed that the flow is enhanced at large separation with  $d = 4.2$  nm when the electric field is applied along the direction aligning with the central axis of DNA. Furthermore, the magnitude of velocity jump in the DNA layer is independent of the channel width. At small separation with  $d = 2.5$  nm, the differences of surface charge distribution and roughness along the  $x$  and  $y$  directions do not influence the flow velocity. The transport behavior of fluid is modified significantly by the ion specificity. For divalent cations,  $Mg^{2+}$  and  $Ca^{2+}$  ions, we study the transport dynamics of fluid based on different parameter sets of force fields. The differences in simulation results suggest that it is necessary to make a correction to interaction parameters between divalent cations and biomolecules. Note that the flow velocity is insensitive to the differences in binding ability for these two kinds of cations based on the original AMBER force field and FFY. In the FFM, the  $Ca^{2+}$  cations bind strongly to DNA leading to largely reduced flow velocity. For monovalent cations, the magnitude of velocity is sorted according to the Hofmeister series. The viscous dissipation induced by flow field becomes dominant compared to the ion-specific effect for cations with weak binding, such as  $Cs^+$ ,  $Rb^+$  and  $K^+$ .

**Acknowledgments** QC gratefully acknowledges support by the Alexander von Humboldt Foundation. This work was also supported by the National Natural Science Foundation of China under Grant No. 31500801.

#### References

- Belkin M, Aksimentiev A (2016) Molecular dynamics simulation of DNA capture and transport in heated nanopores. *ACS Appl Mater Interfaces* 8:12599–12608
- Bell NAW, Engst CR, Ablay M, Divitini G, Ducati C, Liedl T, Keyser UF (2012) DNA origami nanopores. *Nano Lett* 12:512–517
- Berendsen HJC, Postma JPM, van Gunsteren WF, DiNola A, Haak JR (1984) Molecular dynamics with coupling to an external bath. *J Phys Chem* 81:3684–3690
- Berendsen HJC, Grigera JR, Straatsma TP (1987) The missing term in effective pair potentials. *J Phys Chem* 91:6269–6271
- Bonthuis DJ, Netz RR (2012) Unraveling the combined effects of dielectric and viscosity profiles on surface capacitance, electroosmotic mobility, and electric surface conductivity. *Langmuir* 28:16049–16059
- Burns JR, Stulz E, Howorka S (2013) Self-assembled DNA nanopores that span lipid bilayers. *Nano Lett* 13:2351–2356
- Cao Q, Zuo C, Li L, Ma Y, Li N (2010) Electroosmotic flow in a nanofluidic channel coated with neutral polymers. *Microfluid Nanofluid* 9:1051–1062
- Cao Q, Zuo C, Li L, Yang Y, Li N (2011) Controlling electroosmotic flow by polymer coating: a dissipative particle dynamics study. *Microfluid Nanofluid* 10:977–990
- Cao Q, Zuo C, Li L, Zhang Y (2012) Modulation of electroosmotic flow by electric field-responsive polyelectrolyte brushes: a molecular dynamics study. *Microfluid Nanofluid* 12:649–655

- Darden T, York D, Pedersen L (1993) Particle mesh Ewald: an Nlog(N) method for Ewald sums in large systems. *J Phys Chem* 98:10089–10092
- Dekker C (2007) Solid-state nanopores. *Nat Nanotechnol* 2:209–215
- Douglas SM, Marblestone AH, Teerapittayanon S, Vazquez A, Church GM, Shih WM (2009) Rapid prototyping of 3D DNA-origami shapes with caDNAno. *Nucleic Acids Res* 37:5001–5006
- Doyle DA, Cabral JM, Pfuetzner RA, Kuo A, Gulbis JM, Cohen SL, Chait BT, MacKinnon R (1998) The structure of the potassium channel: molecular basis of K<sup>+</sup> conduction and selectivity. *Science* 280:69–77
- Hall AR, Scott A, Rotem D, Mehta KK, Bayley H, Dekker C (2010) Hybrid pore formation by directed insertion of haemolysin into solid-state nanopores. *Nat Nanotechnol* 5:874–877
- Hernández-Ainsa S, Misiunas K, Thacker VV, Hemmig EA, Keyser UF (2014) Voltage-dependent properties of DNA origami nanopores. *Nano Lett* 14:1270–1274
- Hernández-Ainsa S, Keyser UF (2014) DNA origami nanopores: developments, challenges and perspectives. *Nanoscale* 6:14121–14132
- Hess B, Bekker H, Berendsen HJC, Fraaije JGEM (1997) LINC: a linear constraint solver for molecular simulations. *J Comput Chem* 18:1463–1472
- Hess B (2002) Determining the shear viscosity of model liquids from molecular dynamics simulations. *J Chem Phys* 116:209–217
- Hille B (2001) Ion channels of excitable membranes, 3rd edn. Sinauer Associates, Sunderland
- Hou X, Guo W, Jiang L (2011) Biomimetic smart nanopores and nanochannels. *Chem Soc Rev* 40:2385–2401
- Hud NV, Polak M (2001) DNA cation interactions: the major and minor grooves are flexible ionophores. *Curr Opin Struct Biol* 11:293–301
- Humphrey W, Dalke A, Schulten K (1996) VMD: visual molecular dynamics. *J Mol Graph* 14:33–38
- Kasianowicz J, Brandin E, Branton D, Deamer D (1996) Characterization of individual polynucleotide molecules using a membrane channel. *Proc Natl Acad Sci USA* 93:13770–13773
- Kim YW, Netz RR (2006) Electro-osmosis at inhomogeneous charged surfaces: hydrodynamic versus electric friction. *J Chem Phys* 124:114709
- Kowalczyk SW, Wells DB, Aksimentiev A, Dekker C (2012) Slowing down DNA translocation through a nanopore in lithium chloride. *Nano Lett* 12:1038–1044
- Langecker M, Arnaut V, Martin TG, List J, Renner S, Mayer M, Dietz H, Simmel FC (2012) Synthetic lipid membrane channels formed by designed DNA nanostructures. *Science* 338:932–936
- Li AZ, Huang H, Re X, Qi LJ, Marx KA (1998) A gel electrophoresis study of the competitive effects of monovalent counterion on the extent of divalent counterions binding to DNA. *Biophys J* 74:964–973
- Li J, Stein D, McMullan C, Branton D, Aziz MJ, Golovchenko JA (2001) Ion-beam sculpting at nanometre length scales. *Nature* 412:166–169
- Li C-Y, Hemmig EA, Kong J, Yoo J, Hernandez-Ainsa S, Keyser UF, Aksimentiev A (2015) Ionic conductivity, structural deformation, and programmable anisotropy of DNA origami in electric field. *ACS Nano* 9:1420–1433
- Luan B, Aksimentiev A (2008) Electro-osmotic screening of the DNA charge in a nanopore. *Phys Rev E* 78:021912
- Luan B, Aksimentiev A (2010) Electric and electrophoretic inversion of the DNA charge in multivalent electrolytes. *Soft Matter* 6:243–246
- Lyklema J (1995) Fundamentals of interface and colloid science. Academic Press, London
- Mamatkulov S, Fyta M, Netz RR (2013) Force fields for divalent cations based on single-ion and ion-pair properties. *J Chem Phys* 138:024505
- Rothmund PWK (2006) Folding DNA to create nanoscale shapes and patterns. *Nature* 440:297–302
- Rouzina I, Bloomfield VA (1998) DNA bending by small mobile multivalent cations. *Biophys J* 74:3152–3164
- Sakai N, Matile S (2013) Synthetic ion channels. *Langmuir* 29:9031–9040
- Savelyev A, Papoian GA (2006) Electrostatic, steric, and hydration interactions favor Na<sup>+</sup> condensation around DNA compared with K<sup>+</sup>. *J Am Chem Soc* 128:14506–14518
- Schwierz N, Horinek D, Netz RR (2015) Specific Ion binding to carboxylic surface groups and the pH dependence of the Hofmeister series. *Langmuir* 31:215–225
- Seifert A, Gpfrich K, Burns JR, Fertig N, Keyser UF, Howorka S (2015) Bilayer-spanning DNA nanopores with voltage-switching between open and closed state. *ACS Nano* 9:1117–1126
- Sendner C, Horinek D, Bocquet L, Netz RR (2009) Interfacial water at hydrophobic and hydrophilic surfaces: slip, viscosity, and diffusion. *Langmuir* 25:10768–10781
- Simonin J-P, Krebs S, Kunz W (2006) Inclusion of ionic hydration and association in the MSA-NRTL model for a description of the thermodynamic properties of aqueous ionic solutions: application to solutions of associating acids. *Ind Eng Chem Res* 45:4345–4354
- Van Der Spoel D, Lindahl E, Hess B, Groenhof G, Mark AE, Berendsen HJC (2005) GROMACS: fast, flexible, and free. *J Comput Chem* 26:1701–1718
- Wang J, Cieplak P, Kollman PA (2000) How well does a restrained electrostatic potential (RESP) model perform in calculating conformational energies of organic and biological molecules? *J Comput Chem* 21:1049–1074
- Weast RC (1986) CRC handbook of chemistry and physics. CRC Press, Boca Raton
- Yoo J, Wilson J, Aksimentiev A (2016) Improved model of hydrated calcium ion for molecular dynamics simulations using classical biomolecular force fields. *Biopolymers* 105:752–763
- Yoo J, Aksimentiev A (2012) Improved parametrization of Li<sup>+</sup>, Na<sup>+</sup>, K<sup>+</sup>, and Mg<sup>2+</sup> ions for all-atom molecular dynamics simulations of nucleic acid systems. *J Phys Chem Lett* 3:45–50
- Yoo J, Aksimentiev A (2015) Molecular dynamics of membrane-spanning DNA channels: conductance mechanism, electro-osmotic transport, and mechanical gating. *J Phys Chem Lett* 6:4680–4687